Results in coastal waters with high resolution *in situ* spectral radiometry: The Marine Optical System ROV

Mark Yarbrough,[1] Michael Feinholz,[1] Stephanie Flora,[1] Terrance Houlihan,[1] B. Carol Johnson,[2] Yong Sung Kim,[3]
Marilyn Yuen Murphy,[4] Michael Ondrusek,[4] and Dennis Clark[5]
[1]Moss Landing Marine Laboratories, Moss Landing, California
[2]National Institute of Standards and Technology, Gaithersburg, MD
[3]Perot Systems Corporation, Washington, DC
[4]NOAA/NESDIS/STAR, Camp Springs, Maryland
[5]Marine Optical Consulting, Arnold, Maryland

ABSTRACT

The water-leaving spectral radiance is a basic ocean color remote sensing parameters required for the vicarious calibration. Determination of water-leaving spectral radiance using in-water radiometry requires measurements of the upwelling spectral radiance at several depths. The Marine Optical System (MOS) Remotely Operated Vehicle (ROV) is a portable, fiber-coupled, high-resolution spectroradiometer system with spectral coverage from 340 nm to 960 nm. MOS was developed at the same time as the Marine Optical Buoy (MOBY) spectrometer system and is optically identical except that it is configured as a profiling instrument. Concerns with instrument self-shadowing because of the large exterior dimensions of the MOS underwater housing led to adapting MOS and ROV technology. This system provides for measurement of the near-surface upwelled spectral radiance while minimizing the effects of shadowing. A major advantage of this configuration is that the ROV provides the capability to acquire measurements 5 cm to 10 cm below the water surface and is capable of very accurate depth control (1 cm) allowing for high vertical resolution observations within the very near-surface. We describe the integrated system and its characterization and calibration. Initial measurements and results from observations of coral reefs in Kaneohe Bay, Oahu, extremely turbid waters in the Chesapeake Bay, Maryland, and in Case 1 waters off Southern Oahu, Hawaii are presented.

Keywords: CCD, fiber-optic coupled spectrograph, Marine Optical System, ocean color, radiance, Remotely Operated Vehicle, validation, vicarious calibration

1. INTRODUCTION

Various applications utilize ocean color products and have requirements for accurate data from the open ocean and coastal regions, resulting in significant efforts for the calibration and validation of the satellite sensors used for these measurements. NASA's strategic Earth science policy is designed to address critical questions in order to understand how the Earth is changing and what is the potential impact for life [1]. In particular, coastal waters are identified as a top priority question in the Carbon Cycle and Ecosystem Focus Area, where it is necessary to understand whether these regions are a source or a sink of carbon [2]. NOAA utilizes ocean color data in a number of areas, involving the National Ocean Services, the National Marine Fisheries Service, and the Climate Program Office [3, 4, 5]. The data are utilized for operational detection and prediction of harmful algal blooms [6, 7], understanding climate variability, navigation, and fisheries management [8, 9, 10]. The study of coastal ecosystems is important because they are sensitive to climate change and the availability of nutrients. Estuaries and sanctuaries are critical habitats for protected species, where their state is impacted by human activities. Monitoring of their status is the responsibility of NOAA. The Navy utilizes remote sensing from space to support its programs in meteorology and oceanography [11]. Ocean color data, including study of coastal regions, is required for development of products relevant to optical clarity, ocean feature tracking, and coastal ocean physics [12].

In 2007, the SeaWiFS satellite observed its 10-year anniversary of ocean color remote sensing, and the results from this and other satellite sensors are helping to identify future requirements. In ocean color remote sensing, valid and accurate atmospheric correction is essential, because the atmospheric radiance is nominally about 9 times the water-leaving

spectral radiance, $L_w(\lambda)$ for the blue portion of the open ocean spectrum. The aerosol component of the atmospheric correction can be equal in magnitude to $L_w(\lambda)$, making valid atmospheric correction critical. The spectral signature of absorbing aerosols, a common component in coastal regions, can be similar to that of chlorophyll *a*. In coastal regions, the assumption that $L_w(\lambda)$ is zero in the near infrared (NIR), which is a traditional assumption in the atmospheric correction procedure, is no longer valid. It is now known that atmospheric NO_2 absorption can be important for coastal remote sensing in the blue spectral region [13]. Sensors with increased spectral resolution are required for developing improved bio-optical algorithms, as existing model assumptions about the relationships between chlorophyll and colored dissolved organic materials are in question for the open ocean [14]. Because the open ocean is a simple system compared to the complex, coastal waters, high spectral resolution *in situ* radiometry will play a critical role for coastal bio-optical algorithm research. All of these concerns lead to the requirement for future ocean color sensors to have increased spectral information, including ultraviolet (UV) and NIR wavelength coverage with adequate spectral resolution [13].

The uncertainty in derived values of $L_w(\lambda)$ from spacecraft, when traceable to laboratory calibration reference standards with typical combined standard uncertainties of about 3 %, are unacceptably large (~30 %) for derivation of ocean color products. This is a direct consequence of $L_w(\lambda)$ being only about 10 % of the total, at-satellite radiance. This problem is solved through vicarious calibration using *in situ* data under well-defined conditions [15]. The Marine Optical Buoy (MOBY) has functioned in this role, providing accurate, hyperspectral data for 10 years using in-water radiometric techniques [16, 17]. For coastal areas, the primary use of *in situ* data is to validate ocean color products and bio-optical algorithms, as well as to gain a better understanding of the atmospheric correction methodology. For both vicarious calibration and validation, the *in situ* quantity of interest is $L_w(\lambda)$. In-water radiometry requires measurement of the upwelling radiance, $L_u(\lambda)$ at multiple depths, derivation of the attenuation coefficient for $L_u(\lambda)$, followed by propagation through the surface. The in-water light field is quite different for the open ocean and coastal regimes. In the open ocean, termed case 1, the absorption is low and chlorophyll *a* is the primary constituent; in coastal waters the absorption is increased and a variety of dissolved and suspended materials contribute to the optical signature. Hence the optical properties in these case 2 waters are complex, inhomogeneous in the areal and vertical dimensions, and variable in time. For in-water radiometry in these turbid waters, the requirements for assessment of instrument self-shading effects over the complete spectral range, acquisition depth, depth accuracy, and spectral resolution will differ from case 1 waters.

Instrument self-shading is the effect that a portion of the upwelling radiance originates partly in the volume of water that is shadowed by the instrument. This effect becomes significant when the optical depth is of the same order of magnitude as the instrument size. For case 1 waters, where the particle densities are low and the spectral dependence of the absorption of pure water dominates, the effect is least significant in the blue and most significant in the red and NIR spectral regions. In turbid waters, the chlorophyll concentrations, suspended solids and colored dissolved organic matter are so high that absorption in the blue becomes significant and the increased backscattering in the red diminishes the water absorption effects in the water column. This is in sharp contrast with the red-dominated spectral relationship seen in case 1 waters.

Gordon and Ding (1992) used Monte Carlo simulations to estimate the shading effects of instruments on light fields given a set of simplifying assumptions [18]. As an example result, a requirement to limit the bias in $L_u(\lambda)$ to less than 5 % for pure water at 865 nm limited the radius of the profiling instrument to < 1.2 mm. Recent Monte Carlo efforts have expanded the analysis to include systems such as MOS Profiler and MOBY that do not possess azimuthal symmetry [19, 20]. These models require concurrent measurements of spectral absorption and backscattering, which are not always available and contribute significantly to the error budget. The direct way of decreasing the uncertainties is to make the measurements with instruments utilizing optical fibers to reduce the shadowing radius.

Due to the exponential decay of light in the ocean, approximately 95 % of the remotely sensed signal from the oceans originates from the first optical depth. This $1/K_L$ depth, where K_L is the optical attenuation for upwelling radiance, ranges spectrally from tens of meters in clear, case 1 waters to tenths of meters in turbid, case 2 waters. Therefore, the ability to measure just below the surface, and accurately control and maintain the observational depth of the optical sensor is critical. Figure 1 illustrates the bias introduced into $L_w(\lambda)$ for a typical turbid water environment. To examine
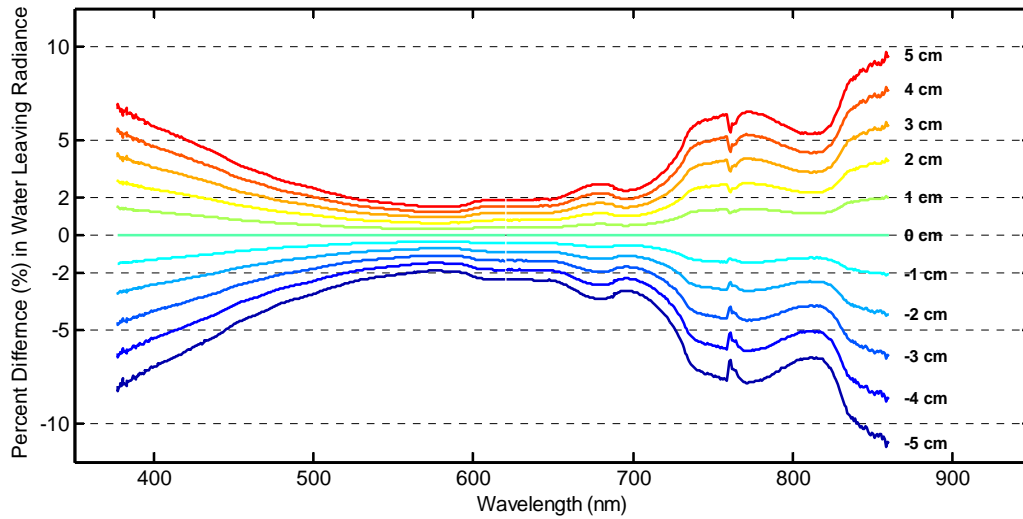
Fig. 1. The bias associated with the determination of the measurement depth for $L_u(\lambda)$ in turbid waters.

the magnitude of the potential depth uncertainty bias, measurements of $L_u(\lambda)$ at two depths were used to calculate $K_L(\lambda)$ and $L_w(\lambda)$. The depth delta was then varied by 1 to 5 cm and the $K_L(\lambda)$ and $L_w(\lambda)$ recomputed to determine the changes in $L_w(\lambda)$ due to the error in depth. This simple calculation illustrates that the depth must be known to 1 cm or better in order to limit the bias to the order of 1 % or less.

The system developed to address these key measurement issues is described and some initial observations are presented in the following sections.

2. MOS Remotely Operated Vehicle (ROV) System Description

MOBY is the primary U.S. facility for vicarious calibration of ocean color satellites [17]. Since the beginning of routine operations in July 1997, over 8365 data sets have been acquired and the results are used to adjust the satellite sensor gain coefficients [21] (for example [16]). The Marine Optical System (MOS) is the optical sensor in MOBY. MOS has two CCD spectrographs that cover the spectral interval from 340 nm to 955 nm [17]. In MOBY, light entering irradiance and radiance collector heads located at different depths or positions are coupled to 1.0 mm silica/silica multimode optical fibers and distributed to a fiberoptic multiplexer. As part of the development of MOBY, an independent system, termed the MOS Profiler, was built. In the MOS Profiler, the submersible instrument housing has UV transmitting window at the $L_u(\lambda)$ port and a cosine collector at the downwelling spectral irradiance, $E_d(\lambda)$, port window; lenses relay the flux to the dichroic beamsplitter followed by the two spectrographs. A mirror is used to select the input: $L_u(\lambda)$ or $E_d(\lambda)$; surface-incident spectral irradiance, $E_s(\lambda)$, data are collected by a separate instrument. The system's primary data acquisition purposes were for additional site characterization at the MOBY position off Lanai, Hawaii, and development of bio-optical algorithms in a variety of waters. The MOS specifications are given in Table 1. The wide dynamic range is a consequence of on-chip binning on the CCD along the slit (spatial) dimension, 16-bit acquisition, and a factor of 3.6×10^6 in integration times.

As configured, the MOS Profiler instrument dimension is 33 cm in diameter and 66 cm in length, with the input window for $L_u(\lambda)$ located off-axis near the outer diameter. The projected shadow diameter is large and variable, depending on the instrument's orientation relative to the sun. For an instrument the diameter of the MOS Profiler, shadowing corrections are necessary at all wavelengths in case 2 waters and in the red and NIR in case 1 waters. In addition, the length and mass of MOS makes it impractical to make observations at depths less than 1 m. In 2003, the Profiler was reconfigured, to be used with a fiber-optical coupling to an ROV. This reconfiguration utilizes a fiber optic relay of its input for $L_u(\lambda)$, fed to the MOS instrument housing on the deck of the ship. The ROV controls the in-water position of

Table 1. The specifications of the MOS are given. A dichroic beamsplitter feeds the input flux to the two spectrographs over the corresponding spectral interval. Except for the input optics and a depolarizer, the system is identical to those used in MOBY.

Parameter	Visible Spectrograph	Near-infrared Spectrograph
Wavelength Range	340 nm – 640 nm	550 nm – 955 nm
Slit Size	25 μm x 12 mm	
F-number	3.8	
Resolution (pixel spacing)	0.58 nm	0.81 nm
Bandpass FWHM	0.91 nm	1.17 nm
Imaging	1:1	
CCD	512 x 512 array, 25 μm pixels, -38°C	
Dynamic Range	$5x10^9$ at SNR of 1000	

the $L_u(\lambda)$ input fiber. Compared to the Profiler, the $L_u(\lambda)$ shadowing diameter is much smaller, less than 5 mm diameter, and the depth control is more precise.

The major change from the MOS Profiler to the MOS ROV configuration involved the input optics at the pressure case and window ports. In the MOS Profiler, the submersible instrument housing was fitted with a window at the $L_u(\lambda)$ port and a cosine collector at the $E_d(\lambda)$ port. The ROV modification involved mounting MOBY 90° radiance collectors at the two MOS ports in a reverse mode of operation. These 90° radiance heads provide some f-number matching and beam expansion in order to better fill the MOS entrance pupil. This adaptation allows the fiber-optic to be directly connected to the radiance head and transmit the light into the MOS window. A schematic of the ROV optical system is shown in Fig. 2.

Two fifty meter, 1 mm diameter, 0.22 NA, silica/silica, multi-mode optical fibers connect the MOS and ROV. These fibers are sheathed in Kelvar and jacketed with PVC. The $L_u(\lambda)$ collector is the polished end of one of the 1 mm diameter optical fibers, mounted in a rigid, steel tubular sheath that is bent 90° for measurements of nadir $L_u(\lambda)$, see Fig. 3. This steel tube is attached to the top of the ROV and extends forward 1 m. The second 50 m fiber has functioned as a spare when the primary fiber was damaged. It has also been utilized with the ROV video system for target selection and alignment during coral work, and for night time operations involving coral fluorescence studies. In these latter applications light sources are coupled to the input end of the fiber via SMA connectors.

In MOS ROV, $E_d(\lambda)$ data are no longer collected, but $E_s(\lambda)$ data are obtained using a MOBY-type $E_s(\lambda)$ straight through collector that is fiber-optic coupled to the MOS instrument in the same manner as the $L_u(\lambda)$ at the other window. This $E_s(\lambda)$ collector is gimbal mounted on the vessel. MOS is secured on deck in an ice bath during all operations in order to maintain a constant ambient temperature and facilitate heat sinking of the internal CCD cooling system.

The ROV is based on the SeaBotix[1] Little Benthic Vehicle (LBV) 150 [22]. Although small, there is adequate power to control the $L_u(\lambda)$ collector in the presence of drag from the umbilical. Power, control, and housekeeping information are transmitted between the ROV and the deck control unit using electrical cables and fiber-optic telemetry that are integrated with the 50 m $L_u(\lambda)$ optical fibers as a single umbilical harness.

The ROV propulsion is based on four independent brushless motor thrusters and efficient nozzles, allowing digital control over the instrument's attitude, position, and velocity. The ROV is equipped with a 525 line resolution camera that is 0.3 lux NTSC video. The camera output is recorded and archived using digital video. Ancillary sensors include a Paroscientific Digiquartz® pressure sensor for depth, Honeywell magnetic heading sensors for attitude, a Tracklink Ultra Short Base Line tracking system for absolute GPS, and Sonar for guidance and obstacle avoidance.

---

[1] Identification of commercial equipment does not imply recommendation or endorsement by the National Institute of Standards and Technology, nor does it imply that the equipment identified is the best available for the purpose.
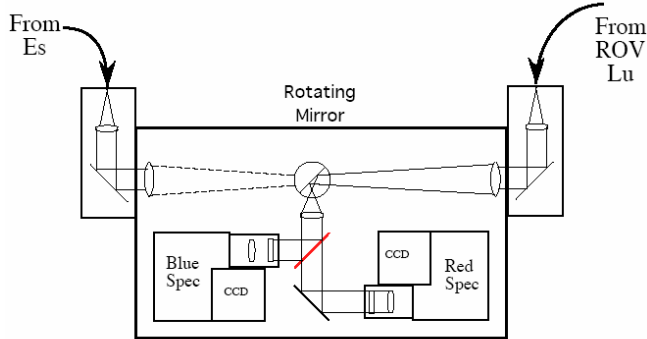
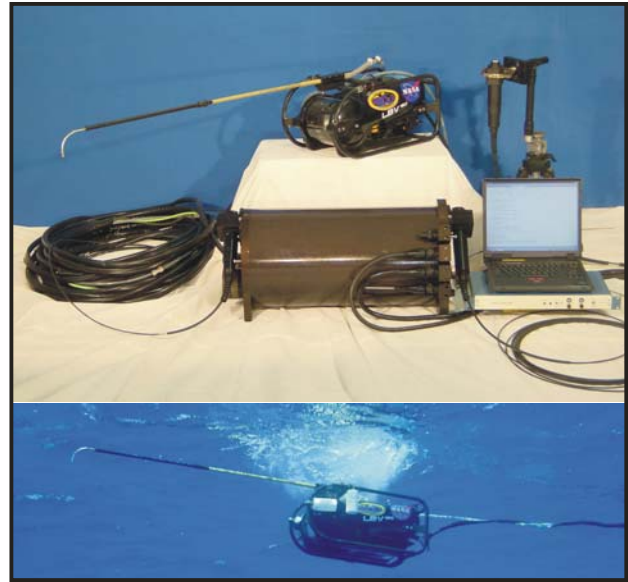Fig. 2. Schematic of the MOS ROV optical system.

Figure 3. MOS ROV system components. The top panel shows the L_u and E_s input fibers and collectors, the ROV, and the ROV control system. The lower panel shows the input fiber for L_u, the ROV, and the optical/electrical umbilical that terminates on deck to MOS and the ROV control system.

Operationally, it is necessary to maintain precise $L_u(\lambda)$ depth control during the measurement integration time and under a variety of sea conditions, e.g. +/- 1 cm is required to maintain 1 % for $L_w(\lambda)$ determinations for turbid waters (see Fig. 1). The ROV's high degree of maneuverability allows for maintaining its orientation to avoid shadowing the measurement and is a benefit during operations that require a variety of instruments to be deployed in the water at the same time. The long umbilical allows for measurements well clear of the ship's shadow.

During operations, the data acquired are binned along the CCD spectrograph slit direction; full images are available for testing and alignment. These data streams are combined in post processing and analyzed using custom MATLAB[2] Moss Landing Marine Laboratories (MLML) database software (MLDBase). This software is GUI-based and has many quality control features. Each scan represents a discrete set of $L_u(\lambda)$ values acquired at the average depth for that scan. Dark scans are acquired before and after each "light" scan using an internal shutter in MOS. The MOS ROV specifications are summarized in Table 2.

The MOS ROV system has been operated in a range of sea conditions. The ROV control starts to degrade when the winds rise above 5.1 m/s (10 knots) – the waves start to build and the boat starts to drag the ROV through the water at a speed greater than the ROV's ability to maintain a stable depth. This is primarily because of surging and pulling on the umbilical.

---

[2] The Mathworks, Inc.

Table 2. The specifications of the MOS ROV are given.

Parameter	Value
Manufacturer	SeaBotix
Model	LBV 150
Chassis dimensions	533 mm L x 320 mm W x 269 mm H
Weight in air	13 kg
L_u standoff distance	1 m
Video camera	530 line, 0.3 lux, color
L_u shadowing diameter	< 5 mm
Azimuth (readout accuracy)	1° (0° to 360°)
Depth control	Wind speed and sea state dependent
Depth resolution	1 mm
Depth control in calm conditions	approximately 1 cm, over 5 cm to 1250 cm depth range
Uncertainty, water temperature	0.1 °C

3. Characterization and calibration

The procedures for the characterization and calibration of the MOS ROV conform to protocols described in NASA Ocean Optics Protocols [23]. Radiometric calibrations are performed before and after each at-sea experiment. Absolute radiometric responsivity is determined from irradiance standards obtained directly from NIST and commercial radiance standards calibrated at NIST. All sources are re-calibrated by NIST at 50 hour lamp burn intervals, and intercomparisons with a NIST transfer radiometer [24] and a portable radiance standard source [25] are performed at yearly intervals. A pair of Standard Lamp Monitors (SLM) designed and built by NIST is used to monitor the irradiance and radiance reference standards at each use between NIST re-calibrations [26]. Additional validation of the MOS ROV radiometric scales is from the second SIMBIOS Radiometric Intercomparison, SIMRIC-2 (August 2002), where the observed differences between expected and measured radiances of MLML sources were within the combined uncertainties of source and transfer radiometer [27].

The wavelength calibration is performed using spectral line emission lamps and its stability is monitored by observation of solar Fraunhofer lines and atmospheric oxygen absorption lines in $E_s(\lambda)$ spectra. An integration time calibration was performed for both spectrographs for exposure times from 0.05 to 100 sec. The stability of the MOS is monitored by an internal reference system of two colored LEDs and an incandescent lamp, reflected by a Spectralon diffuser to the spectrographs. Spectral stray light, or spectral out-of-band, response characterization of the MOS ROV was performed using the NIST SIRCUS facility [28, 29]. The temperature sensitivity for ambient temperature was determined between 3°C and 23°C using a water bath and a stable source. The cosine response of the $E_s(\lambda)$ collector was determined using a laboratory source and rotation and translation stages.

4. *In-situ* results

In order to derive the $L_w(\lambda)$ values that are required inputs for vicarious calibration, product validation, and bio-optical algorithm development, it is necessary to propagate $L_u(z,\lambda)$ through the surface, and this in turn requires determination of $K_L(z,\lambda)$. The approach is summarized here [30]:

$$L_w(\lambda) = L_u(0^-, \lambda)\frac{1-\rho}{n^2},$$

where $L_u(0^-,\lambda)$ is the upwelling spectral radiance just below the surface, ρ is the Fresnel reflectance of the air-sea interface, and n is the index of refraction of seawater. Because of surface winds, waves, and currents, it is not possible to measure $L_u(0^-,\lambda)$ directly. Instead, measurements of $L_u(z,\lambda)$ are made at various depths and $K_L(z,\lambda)$ values are derived according to

$$K_L(z,\lambda) = -\frac{d\ln(L_u(z,\lambda))}{dz} \cong -\frac{\ln(L_u(z+\Delta z,\lambda))-\ln(L_u(z,\lambda))}{\Delta z} = \frac{1}{\Delta z}\ln\left(\frac{L_u(z,\lambda)}{L_u(z+\Delta z,\lambda)}\right)$$

and

$$L_u(0^-, \lambda) = L_u(z, \lambda) \exp\left(\int_0^z K_L(z', \lambda)\, dz'\right).$$

In practice, the $E_s(\lambda)$ data are acquired by a different system which is continuously monitoring the incident irradiance and are used to account for variability in the illumination conditions by normalizing the $L_u(z,\lambda)$ values [17]. If $K_L(z,\lambda)$ is not a strong function of z and we have

$$L_u(0^-, \lambda) \cong L_u(z, \lambda)\, e^{K_L(z,\lambda)\Delta z},$$

where typically the shallowest depth pair is used to determine $K_L(z,\lambda)$ and the shallowest depth $L_u(z,\lambda)$ to evaluate $L_u(0^-,\lambda)$.

We report results of high spectral resolution and near-surface depth determinations of $L_u(z,\lambda)$ with the MOS ROV in clear waters (South of Honolulu, Hawaii, Oahu 7), inorganically and organically dominated turbid waters (the middle of Chesapeake Bay and the Magothy River, Turbid 9), as well as measurements of corals in Kaneohe Bay, Hawaii. The acquisition times and locations are given in Table 3. For the Hawaiian, clear-water (case 1) measurements, $L_u(z,\lambda)$ was measured at 16 depths between 5 cm and 5 m. An average depth increment of 9 cm was used over the first 1.15 m (this varied between 3.5 cm and 17.7 cm) and increasingly larger steps of about 1 m were used down to the final depth of 5 m. For the Chesapeake Bay stations (case 2), $L_u(z,\lambda)$ was measured from 5 cm to 1.5 m in steps of 10 to 40 cm. Environmental conditions during these operations were ideal. The winds were between 2.6 m/s (5 knots) to calm with relatively flat seas permitting excellent control of the ROV. An example of the depth control precision is illustrated in Fig. 4 where the depth sensor data, for Turbid-9 Station 6a, are plotted as a function of time with the observational periods depicted by color. The standard deviations for each mean depth of the 7 depths are listed in the legend. The standard deviations range between 0.5 cm and 2.7 cm and met the requirement for 1 % radiometric uncertainty, e.g., +/- 1 cm, for about 50 % of the depths sampled. The enlarged, inset plot of the surface acquisition of L_u at 0.06 m, shows the actual MOS ROV depth measurement in orange.

MOS ROV results for case 1 waters were acquired southwest (SW) of Oahu, Hawaii (Oahu 7) in March 2005. Figure 5 reports a total of one $E_s(\lambda)$ and 16 $L_u(z,\lambda)$ data sets taken while drifting over a 1 h 40 min interval (Stations 4b and 4c). These data were $E_s(\lambda)$ normalized to the first $E_s(\lambda)$ to remove the incident solar and atmospheric variability. The spectra in the shorter wavelength region typify the magnitude changes for clear water (low attenuation). What is considered significant is the NIR portion, where the normalized $L_u(z,\lambda)$ spectra taken at such small depth sampling increments and over the long sampling interval are internally consistent. These data present a detailed picture of the attenuation process in the upper meter of the water column, e.g. the presence of the atmospheric oxygen A absorption band (758 nm to 778 nm) from 5 cm to about 0.75 m, and the change in slope occurring at and then below 1 m for the spectral region from approximately 780 nm to 820 nm.

Table 3. Details of the profiling radiometric measurements with the MOS ROV.

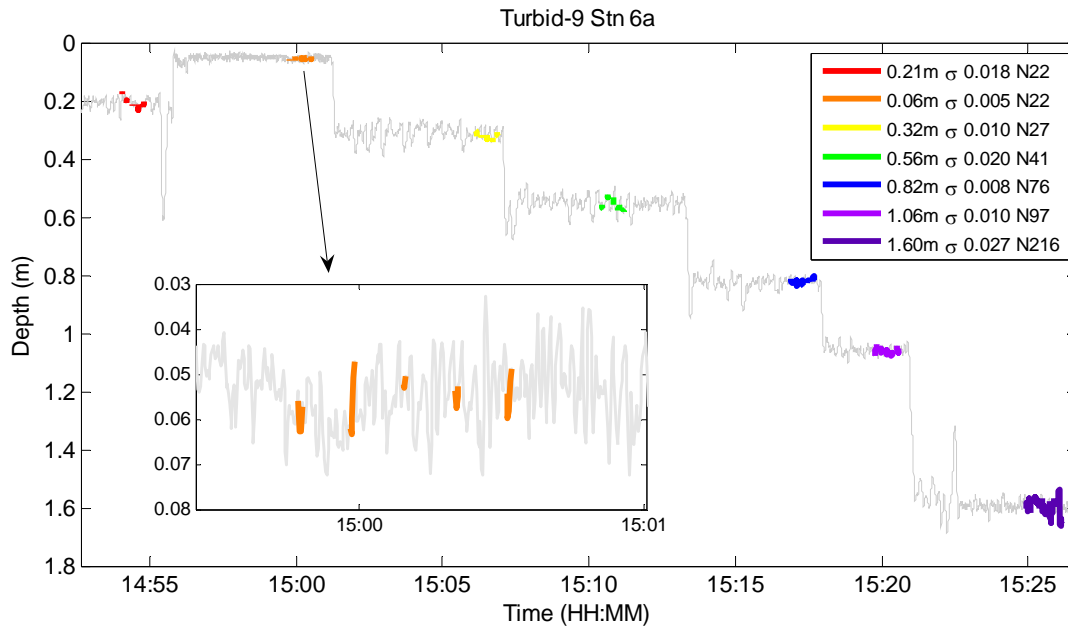| Name	Date	Time	Lat/Long	Location	Chl a mg/m^3
Oahu 7 Station 4b	Mar 17 2005	22:19 GMT	21° 12.4′ N 157° 54.8′ W	SW Oahu	0.10
Oahu 7 Station 4c	Mar 17 2005	00:00 GMT	21° 12.3′ N 157° 53.7′ W	SW Oahu	0.09
Turbid 9 Station 6a	Oct 04 2004	15:00 GMT	39° 6.97′ N 76° 21.03′ W	Chesapeake Bay	7
Turbid 9 Station 26a	Oct 12 2004	14:31 GMT	39° 4.37′ N 76° 29.41′ W	Magothy River	93

Figure 4. Depth sensor readout during Turbid 9. The light gray lines are all the depth data, the colored portions correspond to the full set of MOS ROV acquisition– the inset shows the times corresponding to the L_u scans used in processing.
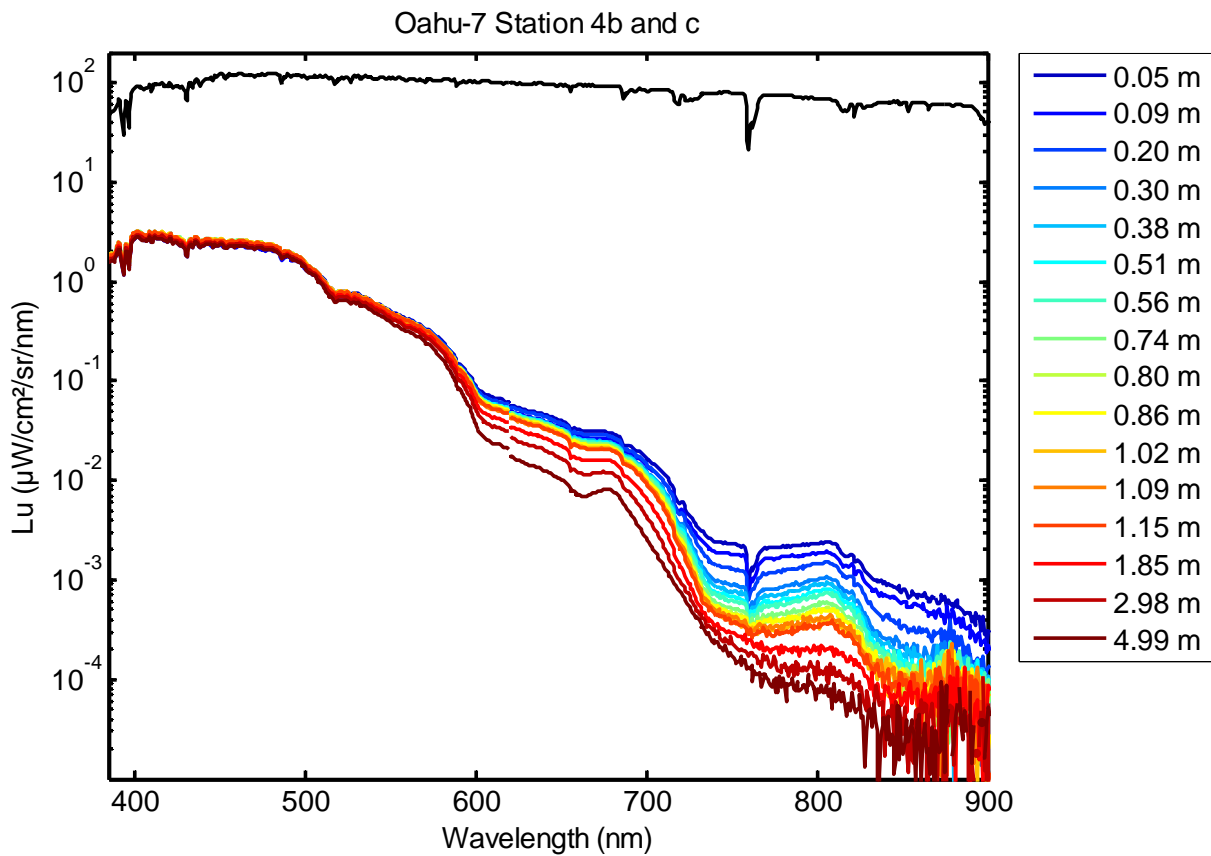

Figure 5. $L_u(z,\lambda)$ depth profile and $E_s(\lambda)$ during Oahu 7 showing spectral coverage by MOS, with a chlorophyll *a* concentration of 0.10 mg/m^3.
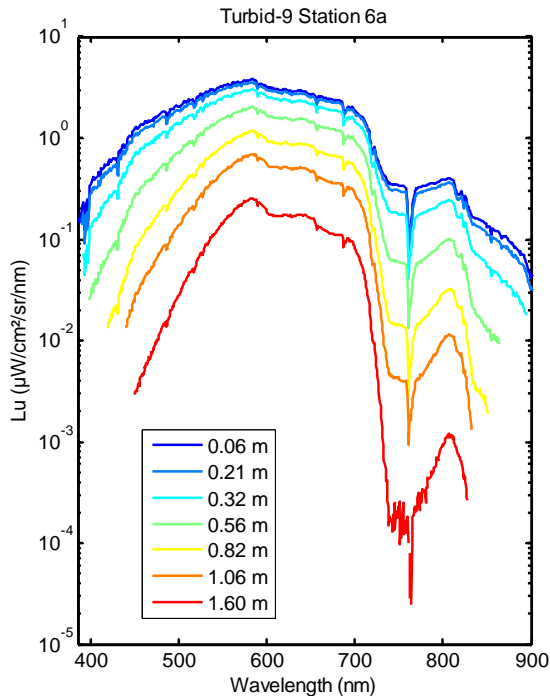
Figure 6. $L_u(z)$ depth profile during Turbid 9, Station 6a, in the middle of the Chesapeake Bay, with a chlorophyll *a* concentration of 7 mg/m^3.
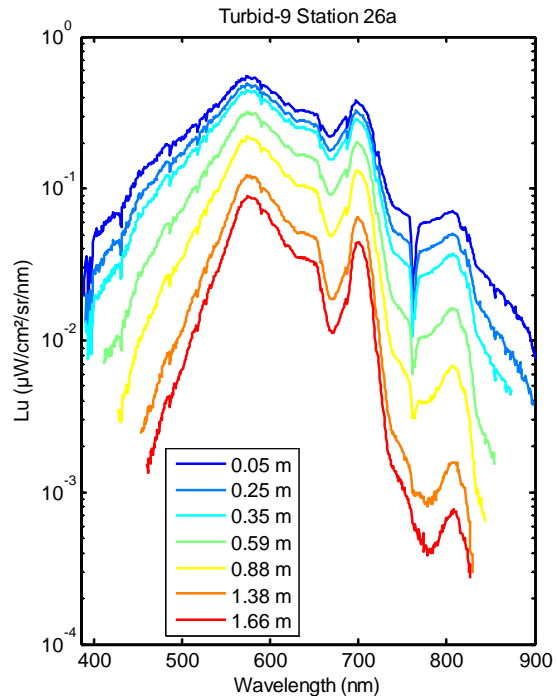
Figure 7. $L_u(z)$ depth profile during Turbid 9, Station 26a, with a chlorophyll *a* concentration of 93 mg/m^3.

Data from the Chesapeake Bay and its Magothy River tributary were acquired in 2004 during an anomalous discharge period following three September hurricanes (Francis, Ivan, and Jeanne), which produced the highest recorded freshwater discharge since 1930 with the average freshwater flow 430 % above the September norm. The heavy sediment flow was confined primarily to the Bay and the entrances to the tributaries. Data acquired in the Bay are shown in Fig. 6, where the chlorophyll *a* was 7 mg/m^3, are typical of the inorganic suspended matter dominated spectral signatures acquired throughout the operational period for Turbid 9 (30 September through 13 October, 2004). In these spectra the elevated levels due to particulate backscattering in the surface layer are most evident at the longer wavelengths.

In clear ocean waters at 650 nm, the upwelled radiance is approximately two orders of magnitude lower than the radiances at 400 nm to 500 nm. In contrast, in these extremely turbid waters the 650 nm radiances are equal too and greater than those shorter wavelengths. $L_u(z,\lambda)$ spectra for a Magothy River station (26a) are presented in Fig. 7. The chlorophyll *a* concentration for these waters was 93 mg/m^3, an order magnitude higher than the Bay station. The effects of these organically dominated waters are evident in the chlorophyll *a* absorption (665 nm) and the chlorophyll fluorescence region (680 nm to 700 nm). Although still elevated by particle backscattering, the effects of water absorption from 570 nm into the NIR for Station 26a are pronounced compared to Station 6a.

Common to both the clear and turbid water observations is the shape of the upwelled spectra in the NIR between 730 nm and 900 nm, where the structure of the incident irradiance is relatively maintained within the first meter. The presence of the oxygen A absorption band still observed at 1.6 m in the extremely high scattering waters of Station 6a in the Chesapeake Bay.
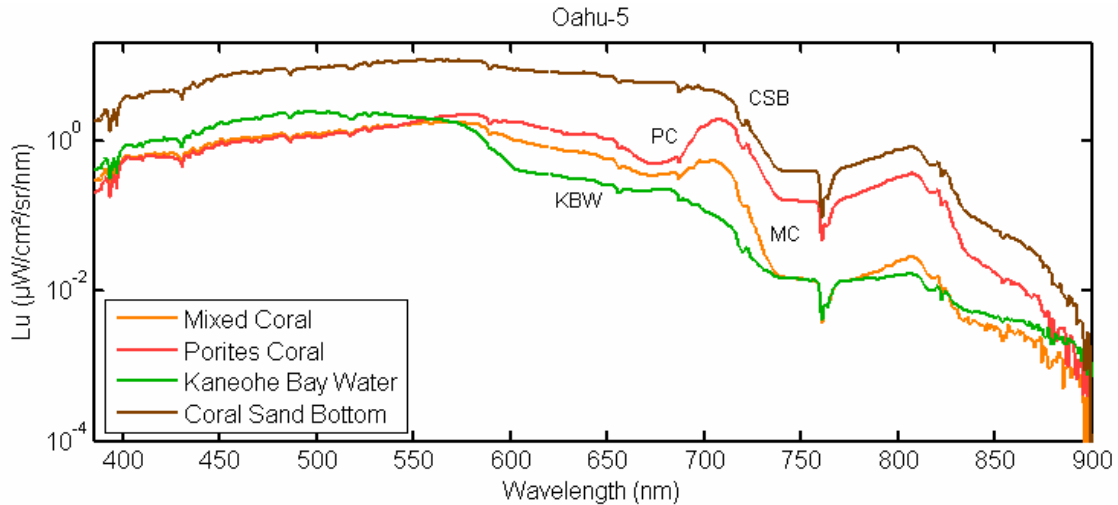
Figure 8. Demostrates the ROV's ability to navigate via the video camera system and maintain a hovering position over a selected coral scene. The upper graph shows the coral spectra, the lower panel shows the video display used during acquisition.

The attributes of the MOS ROV system is further demonstrated in Figure 8, where measurements were conducted in a coral reef environment in Kaneohe Bay, Oahu, Hawaii. The ability to navigate the small ROV via the video camera system and maintain a hovering position over a selected coral scene in very shallow waters provides a capabilitythat would not be possible even with divers. Figure 8 depicts a series of $L_u(z,\lambda)$ measurements pertinent to the interpretation of remotely sensed spectral observations from airborne platforms. The four spectra include a shallow (< 1 m) coral sand bottom, two types of coral targets (mixed types and porites) and the surrounding Kanehoe Bay surface waters. Also, included in Fig. 8 are three coral scenes, recorded from the ROV video camera, while acquiring the $L_u(z,\lambda)$ measurements. The standoff rod containing the optical fiber is visible in the center and right hand images and it is from there that the secondary fiber is used to illuminate the target to provide a visual reference of the target area observed in $L_u(z,\lambda)$. The most prominent spectral feature associated with the coral measurements is the high radiance band around 710 nm. Interpretation of this feature is deferred to knowledgeable scientist in the coral field of study although it is noted that a similar feature is present in the high chlorophyll a (93 mg/m^3) waters of the Magothy River.

5. Summary

We have described a remotely operated hyperspectral radiometric system that meets the requirements demanded for coastal applications of ocean color research. The MOS ROV instrument diameter is less than 5 mm, making it ideally suited for minimizing the effects of instrument self-shading which is required in the red and NIR for case 1 waters and at all wavelengths for case 2 waters. The vertical profile of the instrument is also small, and this allows for measurements just below the surface, which is critical in turbid waters because the upwelled radiance changes rapidly in magnitude and spectral distribution as a function of depth. The precise and accurate depth control of the MOS ROV allows for adequate dwell times to acquire multiple spectra in order to improve the signal-to-noise ratios; incorporation of the video camera ensures the targets measured are those that were selected for study. The broad, high resolution spectral coverage of the MOS is maintained in the MOS ROV; this is essential for the vicarious calibration of ocean

color sensors because their center wavelengths and bandpasses vary with each sensor. The hyperspectral data are also of interest for bio-optical algorithm development and atmospheric correction procedures.

Acknowledgements

REFERENCES

1. Science Plan, http://science.hq.nasa.gov/strategy/Science_Plan_07.pdf
2. Carbon Cycle & Ecosystems Roadmap, http://science.hq.nasa.gov/strategy/roadmaps/carbon.html
3. The Center for Coastal Monitoring and Assessment, http://ccma.nos.noaa.gov
4. Fisheries Data, http://www.nmfs.noaa.gov/gis/data/satellite.htm
5. Climate, http://www.noaa.gov/climate.html
6. R.P. Stumpf, M.E. Culver, P.A. Tester, M. Tomlinson, G.J. Kirkpatrick, B.A. Pederson, E. Truby, V. Ransibrahmanakul, M. Soracco, "Monitoring Krenia brevis blooms in the Gulf of Mexico using satellite ocean color imagery and other data," *Harmful Algae* (**2**), 147-160 (2003).
7. Harmful Algal Bloom Forecasting System, http://csc.noaa.gov/crs/habf
8. Monitoring Phytoplankton Levels, http://www.csc.noaa.gov/crs/rs_apps/issues/seawifs_boston.htm
9. Fisheries and Satellite Data, http://www.pfeg.noaa.gov/~cwilson/fishsat/index.htm
10. Coastal Waters Imaging on GOES-R, http://cioss.coas.oregonstate.edu/CIOSS/Documents/GOESbrochure.pdf
11. The Navy's Needs in Space for Providing Future Capabilities, Committee on the Navy's Needs in Space for Providing Future Capabilities, National Research Council, 266 pp (2005).
12. Naval Research Laboratory Remote Sensing Division, http://rsd-www.nrl.navy.mil/7200/
13. McClain, S. Hooker, G. Feldman, and P. Bontempi, "Satellite data for ocean biology, biogeochemistry, and climate research," *Eos Trans., Am. Geophy. Union*, **87**(34), 337-343 (2006).
14. D.A. Siegel, S. Maritorena, N.B. Nelson, M.J. Behrenfeld, and C.R. McClain, "Colored dissolved organic matter and its influence on the satellite-based characterization of the ocean biosphere," *Geophysical Research Letters*, **32**, L20605, doi:10.1029/2005GL024310 (2005).
15. H.R. Gordon, "In-orbit calibration strategy for ocean color sensors," *Remote Sensing of Environment*, **63**, 265-278 (1998).
16. B.A. Franz, S.W. Bailey, P.J. Werdell, and C.R. McClain, "Sensor-independent approach to the vicarious calibration of satellite ocean color radiometry," *Applied Optics*, **46**(22), 5068-5082 (2007).
17. D.K. Clark, *et al.*, "MOBY, a radiometric buoy for performance monitoring and vicarious calibration of satellite ocean color sensors: measurement and data analysis protocols", *Ocean Optics Protocols for Satellite Ocean Color Sensor Validation, Revision 4*, J.L. Mueller, G.S. Fargion, and C.R. McClain, **Volume 6** , NASA Goddard Space Flight Center, Greenbelt, MD, 3-34 (2003).
18. H.R. Gordon and K. Ding, "Self-shading of in-water optical instruments," *Limnology and Oceanography*, **37(3)**, 491-500 (1989).
19. J.L. Mueller, "Shadow corrections to in-water upwelled radiance measurements: a status review," *Ocean Optics Protocols for Satellite Ocean Color Sensor Validation, Revision 5*, J.L. Mueller, G.S. Fargion and C.R. McClain, **Volume 6**, Part 2, NASA Goddard Space Flight Center: Greenbelt MD, 1-7 (2004).
20. J.L. Mueller, "Self-Shading Corrections for MOBY Upwelling Radiance Measurements, Final Technical Report NOAA Grant NA04NES440007 "Reduced Uncertainties in Measurements of Water-Leaving Radiance, and Other Optical Properties, Using Radiative Transfer Models and Empirical Data Analysis,"" San Diego State University Research Foundation, **33** (2007).
21. Marine Optical Buoy, http://physoce.mlml.calstate.edu/moby/

22. SeaBotix Inc, http://www.seabotix.com/

23. J.L. Mueller and R. Austin, "Characterization of oceanographic and atmospheric radiometers," *Ocean Optics Protocols for Satellite Ocean Color Sensor Validation, Revision 4*, J.L. Mueller, G.S. Fargion and C.R. McClain, Editors., **Volume 2**, NASA Goddard Space Flight Center: Greenbelt MD, 17-33 (2003).

24. B.C. Johnson, S.W. Brown, G.P. Eppeldauer, and K.R. Lykke, "System-level calibration of a transfer radiometer used to validate EOS radiance scales," *Int'l J. Remote Sensing*, **24(2)**, 339-356 (2003).

25. S.W. Brown and B.C. Johnson, "Development of a portable integrating sphere source for the Earth Observing System's calibration validation programme," *Int'l J. Remote Sensing*, **24(2)**, 215-224 (2003).

26. D.K. Clark, M.E. Feinholz, M.A. Yarbrough, B.C. Johnson, S.W. Brown, Y.S. Kim, and R.A. Barnes, "Overview of the radiometric calibration of MOBY," *Proc. SPIE*, **4483**, 64-76 (2001).

27. G. Meister, et al., "The Second SIMBIOS Radiometric Intercomparison (SIMRIC-2), March-November 2002, " NASA/TM-2002-210006, **2**, (2003).

28. M.E. Feinholz, S.J. Flora, M.A. Yarbrough, K.R. Lykke, S.W. Brown, B.C. Johnson, and D.K. Clark, "Stray light correction of the Marine Optical System," *submitted to J. Atmos. Oceanic Tech.* (2007).

29. S.W. Brown, G.P. Eppeldauer, and K.R. Lykke, "Facility for spectral irradiance and radiance responsivity calibrations using uniform sources," *Applied Optics* **45(32)**, 8218-8237 (2006).

30. J.L. Mueller, "In-water radiometric profile measurements and data analysis protocols," *Ocean Optics Protocols for Satellite Ocean Color Sensor Validation, Revision 4,* J.L. Mueller, G.S. Fargion, and C.R. McClain, Editors., **Volume 3**, NASA Goddard Space Flight Center: Greenbelt, MD., 7-20 (2003).